Orbital-Independent Superconducting Gaps in Iron Pnictides

T. Shimojima, *et al.*

Science **332**, 564 (2011);
DOI: 10.1126/science.1202150

28. Y. Xia *et al.*, http://arxiv.org/abs/0812.2078 (2008).
29. T. Ohta, A. Bostwick, T. Seyller, K. Horn, E. Rotenberg, *Science* **313**, 951 (2006).
30. J. H. Jiang, S. Wu, http://arxiv.org/abs/1012.1299v2 (2010).
31. P. Blaha, K. Schwarz, G. Madsen, D. Kvasnicka, J. Luitz, Computer Code WIEN2K (Vienna University of Technology, 2001).
32. P. Roushan *et al.*, *Nature* **460**, 1106 (2009).

33. We acknowledge discussions with M. Neupane, D. Huse, and D. Haldane. Synchrotron x-ray–based measurements are supported by the Office of Basic Energy Sciences, U.S. Department of Energy (grants DE-FG-02-05ER46200, AC03-76SF00098, and DE-FG02-07ER46352). M.Z.H. acknowledges visiting-scientist support from Lawrence Berkeley National Laboratory and additional support from the A. P. Sloan Foundation. Materials growth and characterization are supported by NSF grant DMR-1006492.

Supporting Online Material
www.sciencemag.org/cgi/content/full/science.1201607/DC1
Materials and Methods
SOM Text
Figs. S1 to S18

13 December 2010; accepted 16 March 2011
Published online 31 March 2011;
10.1126/science.1201607

Orbital-Independent Superconducting Gaps in Iron Pnictides

T. Shimojima,[1,2]*† F. Sakaguchi,[1] K. Ishizaka,[1,2] Y. Ishida,[1,3] T. Kiss,[1] M. Okawa,[1] T. Togashi,[4] C.-T. Chen,[5] S. Watanabe,[1] M. Arita,[6] K. Shimada,[6] H. Namatame,[6] M. Taniguchi,[6] K. Ohgushi,[1,3] S. Kasahara,[7] T. Terashima,[7] T. Shibauchi,[8] Y. Matsuda,[8] A. Chainani,[4] S. Shin[1,2,3,4]†

The origin of superconductivity in the iron pnictides has been attributed to antiferromagnetic spin ordering that occurs in close combination with a structural transition, but there are also proposals that link superconductivity to orbital ordering. We used bulk-sensitive laser angle–resolved photoemission spectroscopy on $BaFe_2(As_{0.65}P_{0.35})_2$ and $Ba_{0.6}K_{0.4}Fe_2As_2$ to elucidate the role of orbital degrees of freedom on the electron-pairing mechanism. In strong contrast to previous studies, an orbital-independent superconducting gap magnitude was found for the hole Fermi surfaces. Our result is not expected from the superconductivity associated with spin fluctuations and nesting, but it could be better explained invoking magnetism-induced interorbital pairing, orbital fluctuations, or a combination of orbital and spin fluctuations. Regardless of the interpretation, our results impose severe constraints on theories of iron pnictides.

The high-transition-temperature (T_c) superconducting iron pnictides (*1*) of the $BaFe_2As_2$ (Ba122) family exhibit a typical phase diagram (Fig. 1A) in which the parent compound remains metallic through an antiferromagnetic (AF) spin-ordering transition at T_N and a tetragonal-to-orthorhombic structural transition at T_S (*2*, *3*). Both T_N and T_S decrease in a similar fashion upon ion substitution and lead to an emergent dome-shaped superconducting (SC) phase with a high T_c of up to 55 K (*4*). Such high T_cs are not expected from a conventional electron pairing through lattice vibrations (*5*). Focusing on the nesting tendency connecting quasi-cylindrical Fermi surfaces (FSs), electron pairing mediated by the AF spin fluctuations has been argued (*6*, *7*).

On the other hand, there is a proposal that orbital ordering (*8*–*10*), which causes inequivalency of the Fe *3d* partial density of states, occurs at T_S. This phenomenon could give rise to C2 symmetric physical properties that cannot be expected from only 1% lattice distortion at T_S. In particular, inequivalent occupation of the xz and yz orbitals (x, y, and z represent orthorhombic axes) near the Fermi level (E_F), as observed by angle-resolved photoemission spectroscopy (ARPES), indicates the potential role of orbital degrees of freedom (*11*). Based on the multiorbital nature of iron pnictides, SC pairing through orbital fluctuations has been proposed (*12*–*15*).

Experimental evidence has favored different SC pairing symmetries. Sign-reversal superconductivity suggested by scanning tunneling microscopy on Fe(Te,Se) (*16*) and inelastic neutron spectroscopy on $(Ba,K)Fe_2As_2$ (*17*) is consistent with the s± wave symmetry expected from spin fluctuations. The robustness of T_c against the impurities in LaFeAs(O,F) (*18*) suggests the s++ wave superconductivity, which may be caused by orbital fluctuations. Such material dependence in pairing symmetry can also arise from the balance of these two pairing mechanisms because a crossover from s± to s++ symmetry may occur, depending on the strengths of microscopic electronic parameters (*12*–*15*). However, to date there has been no experimental evidence for the role of orbital fluctuations on the superconductivity in the pnictides.

The pairing mechanism will be reflected in the momentum dependence of the SC gap properties. Spin fluctuation mechanism predicts strongly orbital-dependent SC gap magnitude (*7*, *19*), but orbital fluctuations should eliminate such orbital dependence (*13*–*15*). Because each FS sheet in iron pnictides has a distinct d-orbital character, probing the FS dependence of the SC gap magnitude will be a crucial test for identifying the contribution of the orbital fluctuations in the electron pairing. Here, we report the FS dependence of the SC gap magnitude of representative iron-pnictide superconductors $BaFe_2(As_{0.65}P_{0.35})_2$ (AsP122) and $Ba_{0.6}K_{0.4}Fe_2As_2$ (BaK122) by using bulk-sensitive laser-ARPES (*20*) [see section 1 of the supporting online material (SOM)].

ARPES, using a fixed photon energy (hν), probes a specific profile of the in-plane FSs perpendicular to the momentum axis along the z direction k_z. Especially for AsP122 with strong FS warping, the orbital character depends on the k_z value (*21*). Estimation of k_z value corresponding to 7 eV photons of laser-ARPES is thus necessary for investigating the orbital dependence of the SC gap magnitude. Figure 1B is a schematic of the experimental FS profile along the k_z axis of AsP122 taken from (*22*). Whereas the inner hole FS is almost cylindrical, the outer one gets enlarged toward $k_z = \pi$, consistent with the band calculations (inset of Fig. 1A) (*21*). We used a synchrotron radiation photon source of 10 eV and 7 eV to find this characteristic warping in the inner (k_{F1}) and outer (k_{F2}) Fermi momenta. As shown in Fig. 1, C and D, separation between k_{F1} and k_{F2} in C was three-fourths of that in D, which indicates that 7 eV photons probe the FS profile at $k_z \sim \pi$ to 1.2π. This estimate of k_z for $h\nu = 7$ eV was also quantitatively confirmed by the comparable FS size obtained by the higher photon energy of 63 eV probing $k_z \sim \pi$ (*22*) (Fig. 1E).

High-resolution laser-ARPES *E*-*k* images for AsP122 (Fig. 2, B and C) are along cut 1 and 2 indicated in Fig. 2A, respectively. Both the inner and middle hole bands were resolved as the two-peak feature in the momentum distribution curve (MDC) near E_F (Fig. 2B), although they are nearly degenerate in Fig. 1, C and D. We could separate three hole bands along cut 1 and 2. The temperature (*T*) dependence of the energy distribution curves (EDCs) at k_F in cut 2 (outer FS) shows the SC gap opening below bulk T_c (Fig. 2D), and the SC gap magnitude Δ was directly extracted from the fitting procedure using a Bardeen-Cooper-Schrieffer (BCS) spectral function (SOM, section 2). This Δ value is in excel-

[1]Institute for Solid State Physics (ISSP), University of Tokyo, Kashiwa, Chiba 277-8581, Japan. [2]Japan Science and Technology Agency (JST), Core Research for Evolutional Science and Technology (CREST), Chiyoda-ku, Tokyo 102-0075, Japan. [3]JST, Transformative Research Project on Iron Pnictides, Chiyoda-ku, Tokyo 102-0075, Japan. [4]RIKEN SPring-8 Center, Sayo, Hyogo 679-5148, Japan. [5]Beijing Center for Crystal Research and Development, Chinese Academy of Science, Zhongguancun, Beijing 100190, China. [6]Hiroshima Synchrotron Radiation Center and Graduate School of Science, Hiroshima University, Hiroshima 739-8526, Japan. [7]Research Center for Low Temperature and Materials Sciences, Kyoto University, Sakyo-ku, Kyoto 606-8501, Japan. [8]Department of Physics, Kyoto University, Sakyo-ku, Kyoto 606-8502, Japan.

*Present address: Department of Applied Physics, Graduate School of Engineering, University of Tokyo.
†To whom correspondence should be addressed. E-mail: shimojima@ap.t.u-tokyo.ac.jp (T.S); shin@issp.u-tokyo.ac.jp (S.S.)

lent agreement with the BCS-like T dependence (inset of Fig. 2D). Figure 2, E to G, shows EDCs in the SC state and fitting results for each hole FS. A shift in the leading edge relative to E_F indicates an SC gap opening. As shown in Fig. 2H, the FS angle dependence of Δ indicates the fully gapped nature of the three hole FSs in AsP122. Considering the nodal SC gap symmetry proposed by the magnetic penetration depth, thermal conductivity (*23*) and nuclear magnetic resonance measurements (*24*), our results rule out d-wave symmetry and imply the possible presence of line nodes in electron FSs around zone corners. The Δ of each hole FS is comparable to the common reduced gap value of $2\Delta/k_BT_c \sim 3.0$.

The laser-ARPES results on BaK122 (Fig. 3A) showed three hole FSs around the zone center, which is consistent with the first-principles band calculations with experimental lattice constants. We separately observed the three hole bands by varying the laser polarizations. Figure 3B shows the three hole bands measured by circular polarization along the momentum cut represented by the white arrow in Fig. 3A. When we chose p-polarization, the band A became dominant (Fig. 3C), in contrast to the band B and C being active in s-polarization (Fig. 3D). Such strong polarization dependence of the photoelectron intensity implies a different d-orbital character in these hole bands (*11*). We make use of the

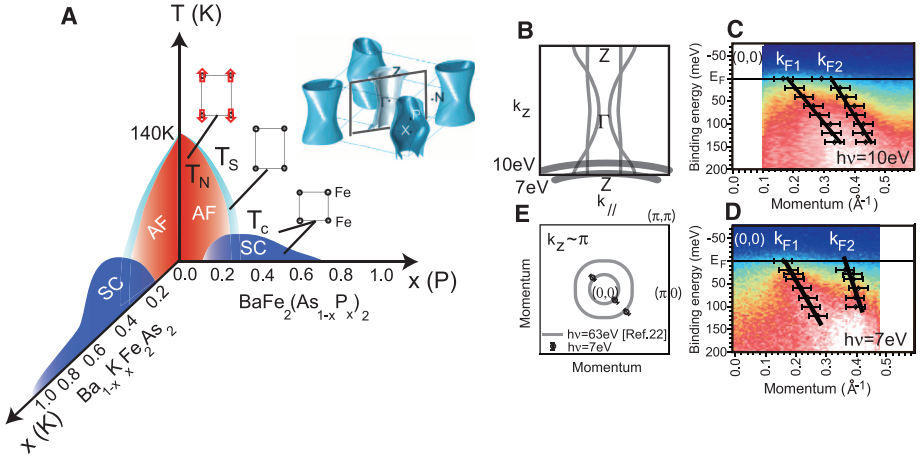

Fig. 1. (**A**) Schematic phase diagram of $BaFe_2(As,P)_2$ and $(Ba,K)Fe_2As_2$. T_N represents the AF transition temperature and T_S a tetragonal to orthorhombic structural transition temperature. Red arrows indicate stripe-type AF spin ordering on the orthorhombic lattice. Inset shows calculated FSs of optimally doped $BaFe_2(As,P)_2$. (**B**) Momentum cut along k_z axis corresponding to the gray rectangle in the inset of (A). FS profile of $BaFe_2(As,P)_2$ reported in (*22*) is indicated by the gray curve. (**C** and **D**) Hole band dispersions around the zone center measured by synchrotron radiation photon sources of hν = 10 eV and 7 eV, respectively. Inner (k_{F1}) and outer (k_{F2}) Fermi momenta are estimated by plotting the peak positions of MDCs below E_F. Comparing the k_F dispersions along the k_z axis (*22*), momentum cuts measured by hν = 7 eV and 10 eV are superimposed as black curves at the bottom of (B). (**E**) Quantitative comparison of the k_F measured by hν = 7 eV and 63 eV, indicating reliable determination of $k_z = \pi$. Black circles represent k_{F1} (nearly degenerate inner and middle hole bands in Fig. 2B) and k_{F2} (outer hole band in Fig. 2C) obtained by synchrotron radiation photon source of hν = 7 eV. The gray curve represents FSs obtained by hν = 63 eV (*22*).

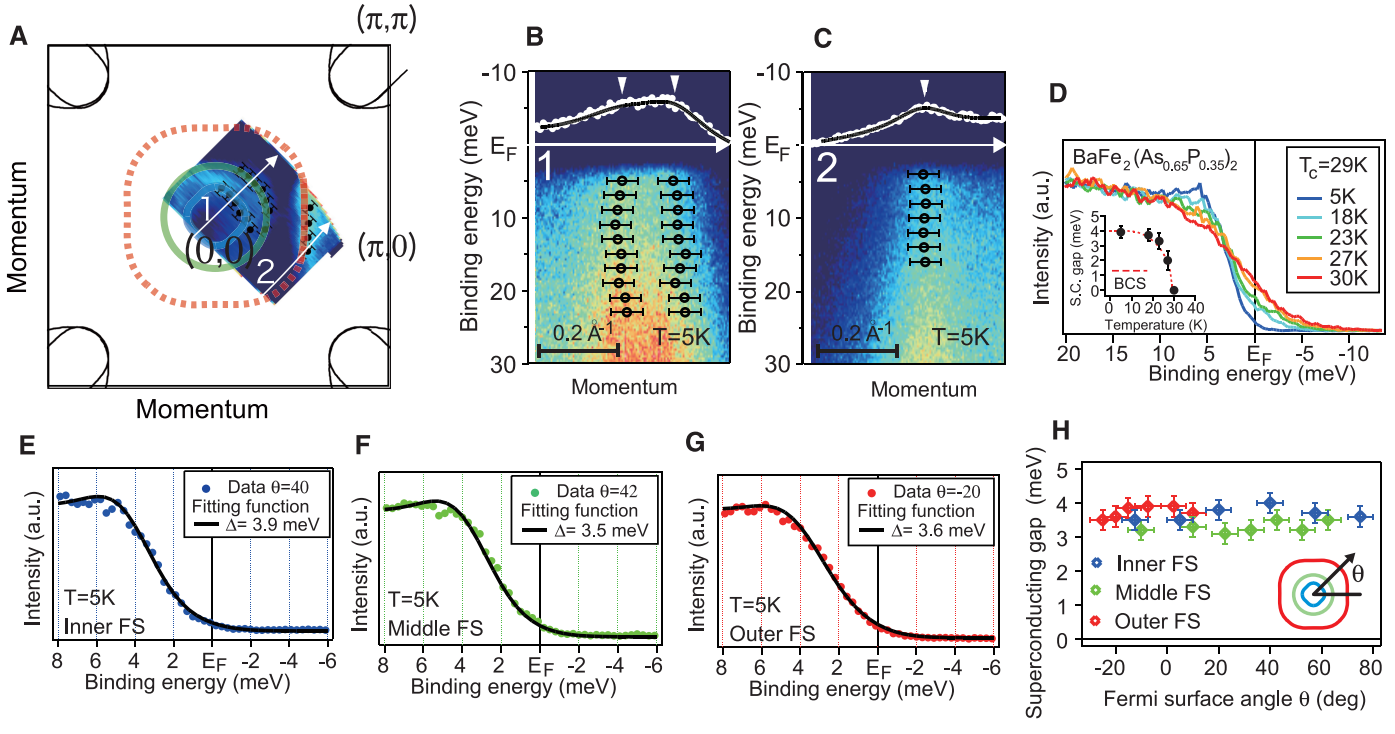

Fig. 2. Laser-ARPES on $BaFe_2(As_{0.65}P_{0.35})_2$. (**A**) FSs around the (0,0) point of $BaFe_2(As_{0.65}P_{0.35})_2$, measured by circularly polarized laser. (**B** and **C**) Band dispersions measured by circular polarization along cut 1 and cut 2 in (A), respectively. (**D**) T dependence of EDC at k_F in cut 2. Inset shows T dependence of the SC gap magnitude determined by the fitting procedure, using the BCS spectral function. The red broken curve represents BCS-like T dependence. (**E** to **G**) Fitting results on the EDCs in the SC state measured at k_F of inner, middle, and outer FS, respectively. (**H**) FS angle dependence of the SC gap magnitude in each hole FS. Inset shows the definition of the FS angle θ.

polarization dependence for separating band A from others to discuss its T dependence across T_c.

In Fig. 3E, we show the T dependence of the EDC at k_F of band A measured with a p-polarized laser. A distinct two-peak structure (peak 1 and peak 2) was observed near E_F with decreasing T. To emphasize the peak 1′ in the unoccupied state, we divided EDCs using a Fermi Dirac (FD) function convoluted by a Gaussian corresponding to the experimental energy resolution. Divided spectra were further normalized by that measured at 60 K (Fig. 3F). Both peaks 1 and 1′ appeared just below bulk T_c, accompanying a gap structure centered at E_F consistent with the Bogoliubov quasiparticle picture. This observation strongly suggests that peaks 1 and 1′ arise from superconductivity. However, peak 2 is found even in the normal state, which suggests that it is a non-SC peak (for its detailed analysis and possible origin, see SOM section 3).

We can quantitatively estimate Δ for each hole FS sheet focusing on the peak 1 and gap structure around E_F in a similar manner to that used for AsP122. By extracting the SC gap magnitude from a series of T-dependent EDCs in Fig. 3E, an excellent agreement with BCS-like T dependence is obtained as shown in Fig. 3G. Figure 3, H to J, shows the EDCs in the SC state and the fitting results for each hole FS in BaK122. As indicated by the leading-edge shift in EDCs at FS angles θ = 8 and θ = 45 degrees (Fig. 3H), we observed slight anisotropy in Δ. The definition of the FS angle θ and the gap anisotropy in each hole FS is summarized in Fig. 3K. In addition to the fully gapped nature, we found comparable Δ values for the three hole FSs with a small reduced gap value of $2\Delta/k_BT_c \sim 1.7$ (SOM, section 4) This result is in a strong contrast to the "two-gap" picture previously observed at around zone center (*25*, *26*) (SOM, section 5).

The FS-sheet dependences of SC gap magnitude in AsP122 and BaK122 obtained by laser-ARPES are summarized in Fig. 4. The most remarkable feature commonly observed in AsP122 and BaK122 is the coincidence of Δ in the three hole FSs. At least for AsP122, the size and this characteristic behavior in SC gaps are observed independently of the k_z values (SOM, section 6) First-principles band calculations indicate that each hole FS is characterized by a different orbital character. This property was also experimentally confirmed by the strong polarization dependence in hole bands of BaK122 (Fig. 3, B to D). The comparable Δ for all hole FSs thus indicate that they are almost orbital-independent.

Of course, conventional isotropic electron-phonon interaction can give a homogeneous Δ for all FSs, but this mechanism is not likely in iron pnictides for three reasons. First, high T_c up to 55 K (*4*) is not expected from the conventional electron-phonon interactions (*5*). Second, a nodal SC gap is experimentally suggested in several iron pnictides (*23*, *24*, *27*, *28*). Third, material dependence of the SC gap magnitude implies electron-pair scattering between hole and electron FSs, originating in the FS nesting (SOM, section 7). We expect that the pairing mechanism is not purely of phonon mediation but is closely related to the spin fluctuations and/or orbital fluctuations. For a spin-fluctuations pairing mechanism (*6*, *7*, *19*), the SC gap is most closely related to the spin susceptibility. The calculated spin susceptibility suggests dominant electron-pair scattering between disconnected FSs composed of the same orbital character (*7*, *19*) (intraorbital pairing), as illustrated in Fig. 4B. Then, Δ is expected to be highly sensitive to the orbital character, depending on the overlap of the FS shape it composes. This property, nevertheless, contradicts the orbital-insensitive SC gaps we observed in the laser-ARPES experiments.

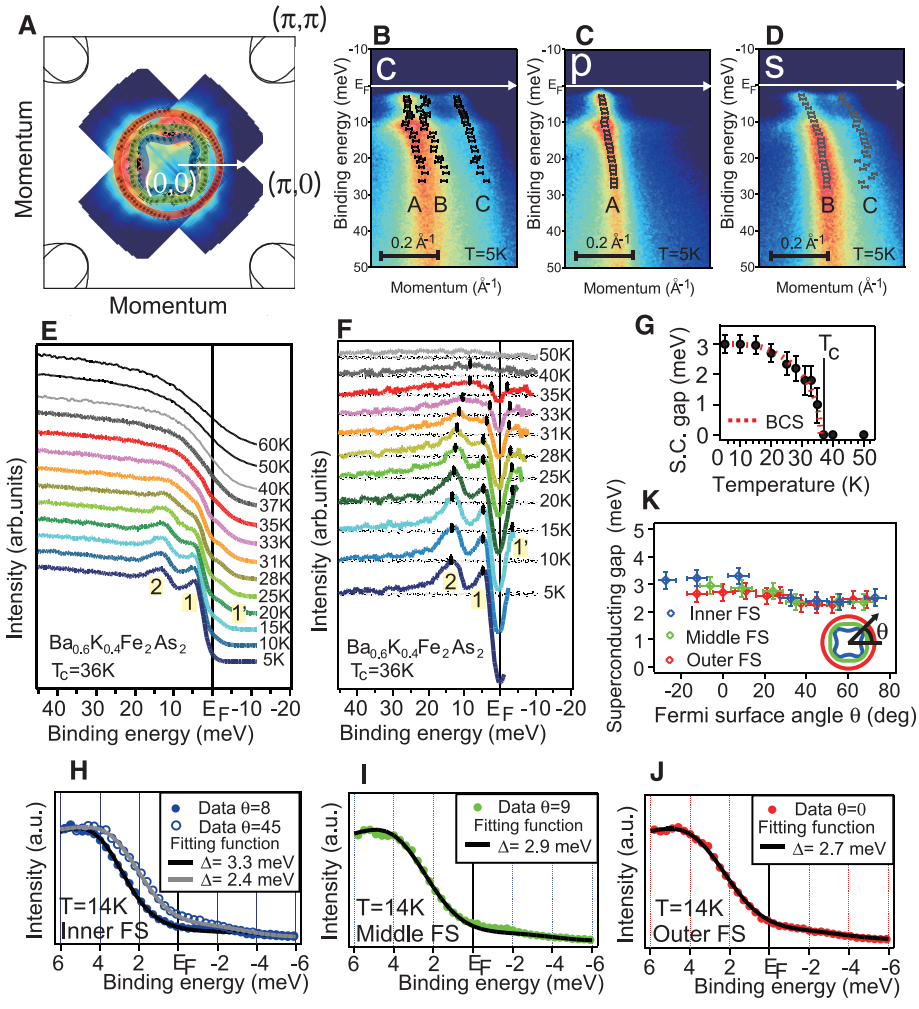

Fig. 3. Laser-ARPES on $Ba_{0.6}K_{0.4}Fe_2As_2$. (**A**) FSs around the (0,0) point of $Ba_{0.6}K_{0.4}Fe_2As_2$, measured by circularly polarized laser. (**B** to **D**) Band dispersions measured by circular, p-, and s- polarized laser, respectively. The corresponding momentum cut is shown by the white arrow in (A). (**E**) T dependence of EDC at k_F of band A, measured by p-polarization. The contribution from other hole bands is already removed by choosing polarization, and the spectral weight at E_F is very low, indicative of the clear SC gap opening. (**F**) EDCs divided by FD functions. They are further normalized by the divided EDC at 60 K to extract the T-dependent component. Black dots represent the peak position of peak 1, peak 1′ and peak 2. (**G**) T dependence of the SC gap magnitude estimated by fitting analysis using the BCS spectral function. The red broken curve represents BCS-like T dependence. (**H** to **J**) Fitting results on the EDCs in the SC state, measured in inner, middle, and outer FS, respectively. (**K**) FS angle dependence of the SC gap magnitude in each hole FS. Inset shows the definition of the FS angle θ.

In particular, we focus on the $3Z^2$-R^2 (X, Y, and Z represent tetragonal axes) orbital because it does not contribute to the electron FSs around zone corners in 122 systems (Fig. 4, C and D) (*21*). In this case, intraorbital electron pairing between the disconnected FSs is suppressed, and then the Δ of the $3Z^2$-R^2 orbital electrons should be quite small. According to the band calculations in (*21*), the $3Z^2$-R^2 orbital is dominant in the outer hole FS of AsP122 around $k_z \sim \pi$. This is supported by our polarization-dependent laser-ARPES, which shows a dominantly $3Z^2$-R^2 orbital character in the outer hole FS of AsP122 (SOM, section 8). Taking this into account, the comparable size of SC gap magnitude for various orbital characters, including the $3Z^2$-R^2 orbital,

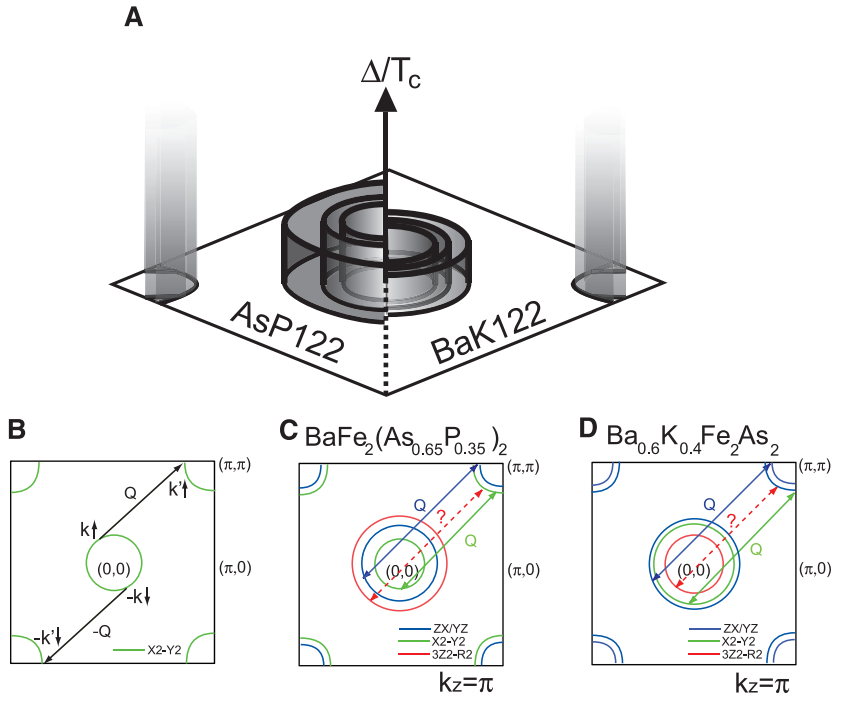

Fig. 4. (**A**) Schematic momentum dependence of the superconducting gap magnitude around $k_z = \pi$ in $BaFe_2(As_{0.65}P_{0.35})_2$ and $Ba_{0.6}K_{0.4}Fe_2As_2$, determined by laser-ARPES. Those in electron FSs around zone corners (light gray) are speculations. (**B**) Illustration of the electron pair scattering from (k↑,-k↓) to (k′↑,-k′↓) between disconnected FSs of the same orbital character (intraorbital pairing). Electrons are scattered by the AF spin fluctuations with the wave vector Q derived from the FS nesting. (**C** and **D**) Schematic FS profiles at $k_z = \pi$ for AsP122 and BaK122, respectively. The number of FS sheets and their orbital characters are based on the first-principles band calculations using experimental atomic positions of $x = 0.4$ ($x = 0.33$) for BaK122 (AsP122) with $BaFe_2As_2$ structure. FS sheets composed of ZX/YZ, X^2-Y^2, and $3Z^2$-R^2 orbitals (X, Y, and Z represent tetragonal axes) are colored in blue, green, and red, respectively. Arrows with wave vector Q represent the nesting tendency between FS sheets of the same orbital character. Because $3Z^2$-R^2 orbital electrons do not form the FSs around zone corners, they cannot participate in electron pairing through the spin fluctuations of wave vector ~ Q (*15*, *30*).

can hardly be explained by the spin-fluctuation mechanism alone.

However, the importance of interorbital coupling (*29*, *30*) and the role of the orbital fluctuations are being theoretically raised (*12*–*15*), which has been neglected in the genuine spin-fluctuations pairing mechanism. Such interorbital electron pairing is expected to dissolve the orbital dependence of Δ and can explain the comparable Δ around the zone center observed by laser-ARPES.

A multiorbital band structure near E_F in iron pnictides has the potential to enhance the orbital fluctuations. In addition, orbital fluctuations are expected to evolve in the vicinity of the orbital ordered state. In the parent material of iron pnictides, antiferromagnetic ordering generally occurs accompanying the structural transition from tetragonal to orthorhombic crystal symmetry (*2*, *3*) (Fig. 1). Recently, orbital ordering at the structural transition was theoretically proposed (*8*–*10*). Previous laser-ARPES on Ba122 reported unequal occupation in the electronic structure of zx and yz orbitals below the magneto-structural transition supporting the possible orbital ordering scenario (*11*). In addition, the spin and orbital degrees of freedom might be strongly coupled for the parent and superconducting compounds (*31*–*35*). Theoretical studies have shown that superconductivity in the iron pnictides could be derived from orbital fluctuations mixed with spin fluctuations (*31*, *35*). Considering this background, the present result is reasonably explained as an indication of the importance of orbital fluctuations for the superconductivity of the iron pnictides; this should be taken into account at least on the same footing as spin fluctuations. Thus, while a dominantly orbital-fluctuation–derived superconductivity can be somewhat speculative and needs to be confirmed by further work, our results clearly provide severe constraints for a complete theory of superconductivity in the iron pnictides.

References and Notes

1. Y. Kamihara, T. Watanabe, M. Hirano, H. Hosono, *J. Am. Chem. Soc.* **130**, 3296 (2008).
2. S. Kasahara *et al.*, *Phys. Rev. B* **81**, 184519 (2010).
3. M. Rotter, M. Tegel, D. Johrendt, *Phys. Rev. Lett.* **101**, 107006 (2008).
4. Z. Ren *et al.*, *Chin. Phys. Lett.* **25**, 2215 (2008).
5. L. Boeri, O. V. Dolgov, A. A. Golubov, *Phys. Rev. Lett.* **101**, 026403 (2008).
6. I. I. Mazin, D. J. Singh, M. D. Johannes, M. H. Du, *Phys. Rev. Lett.* **101**, 057003 (2008).
7. K. Kuroki *et al.*, *Phys. Rev. Lett.* **101**, 087004 (2008).
8. F. Krüger, S. Kumar, J. Zaanen, J. V. Brink, *Phys. Rev. B* **79**, 054504 (2009).
9. W. Lv, J. Wu, P. Phillips, *Phys. Rev. B* **80**, 224506 (2009).
10. C. C. Lee, W.-G. Yin, W. Ku, *Phys. Rev. Lett.* **103**, 267001 (2009).
11. T. Shimojima *et al.*, *Phys. Rev. Lett.* **104**, 057002 (2010).
12. J. Zhang, R. Sknepnek, R. M. Fernandes, J. Schmalian, *Phys. Rev. B* **79**, 220502R (2009).
13. H. Kontani, S. Onari, *Phys. Rev. Lett.* **104**, 157001 (2010).
14. Y. Yanagi, Y. Yamakawa, Y. Ōno, *Phys. Rev. B* **81**, 054518 (2010).
15. T. Saito, S. Onari, H. Kontani, *Phys. Rev. B* **82**, 144510 (2010).
16. T. Hanaguri, S. Niitaka, K. Kuroki, H. Takagi, *Science* **328**, 474 (2010).
17. A. D. Christianson *et al.*, *Nature* **456**, 930 (2008).
18. M. Sato *et al.*, *J. Phys. Soc. Jpn.* **79**, 014710 (2010).
19. K. Kuroki, H. Usui, S. Onari, R. Arita, H. Aoki, *Phys. Rev. B* **79**, 224511 (2009).
20. Materials and methods are available as supporting material on *Science* Online.
21. K. Suzuki, H. Usui, K. Kuroki, *J. Phys. Soc. Jpn.* **80**, 013710 (2011).
22. T. Yoshida *et al.*, *Phys. Rev. Lett.* **106**, 117001 (2011).
23. K. Hashimoto *et al.*, *Phys. Rev. B* **81**, 220501 (2010).
24. Y. Nakai *et al.*, *Phys. Rev. B* **81**, 020503R (2010).
25. H. Ding *et al.*, *Europhys. Lett.* **83**, 47001 (2008).
26. D. V. Evtushinsky *et al.*, *Phys. Rev. B* **79**, 054517 (2009).
27. J. D. Fletcher *et al.*, *Phys. Rev. Lett.* **102**, 147001 (2009).
28. J.-Ph. Reid *et al.*, *Phys. Rev. B* **82**, 064501 (2010).
29. A. Moreo, M. Daghofer, A. Nicholson, E. Dagotto, *Phys. Rev. B* **80**, 104507 (2009).
30. A. F. Kemper *et al.*, *N. J. Phys.* **12**, 073030 (2010).
31. T. D. Stanescu, V. Galitski, S. Das Sarma, *Phys. Rev. B* **78**, 195114 (2008).
32. S. Nandi *et al.*, *Phys. Rev. Lett.* **104**, 057006 (2010).
33. S.-H. Lee *et al.*, *Phys. Rev. B* **81**, 220502R (2010).
34. M. Daghofer *et al.*, *Phys. Rev. B* **81**, 180514R (2010).
35. M. Daghofer, A. Nicholson, A. Moreo, E. Dagotto, *Phys. Rev. B* **81**, 014511 (2010).

Acknowledgments: We thank W. Malaeb for experimental supports and valuable discussions. We acknowledge T. Yoshida, R. Arita, H. Kontani, S. Onari, M. Ogata, and Y. Yanase for valuable discussions. We acknowledge K. Kuroki, H. Usui, Y. Suzuki, and A. Carrington for valuable discussions and first-principles band calculations. Part of this work was performed at the Hiroshima Synchrotron Radiation Center, Hiroshima university, Japan (proposal 10-B-24). Support for this work was provided by Special Coordination Funds for Promoting Science and Technology, Promotion of Environmental Improvement for Independence of Young Researchers (to K.O.). This research is supported by the Japan Society for the Promotion of Science (JSPS) through its Funding Program for World-Leading Innovative R&D on Science and Technology (FIRST) Program.

Supporting Online Material

www.sciencemag.org/cgi/content/full/science.1202150/DC1
Materials and Methods
SOM Text
Figs. S1 to S4
References

23 December 2010; accepted 22 March 2011
Published online 7 April 2011;
10.1126/science.1202150